Microelectronic Engineering 238 (2021) 111511

Contents lists available at ScienceDirect

Microelectronic Engineering

journal homepage: www.elsevier.com/locate/mee

Research paper

Flexible transparent conductive electrode of Au/PDMS prepared by electrochemical-assisted peeling

Gang Wang [a], Yufei Zhai [b,c], Chenghao Lv [a], Wenjing Fan [b,c], Cong Zhao [b,c], Min Wang [b,c,*]

[a] Department of Mechanics and Aerospace Engineering, Southern University of Science and Technology, Shenzhen 518055, China
[b] School of Microelectronics, Southern University of Science and Technology, Shenzhen 518055, China
[c] Engineering Research Center of Integrated Circuits for Next-Generation Communications, Ministry of Education, Southern University of Science and Technology, Shenzhen 518055, China

ARTICLE INFO

Keywords:
Transparent conductive electrode
Metal grid
Electrochemical-assisted peeling
Sheet resistance
Transmittance

ABSTRACT

Metal grids have great potential in flexible transparent conductive electrodes (*E*-TCEs) due to their high conductivity and transparency. Unlike other TCEs, the sheet resistance and optical transmittance of metal grids can be independently adjusted. However, the large surface roughness resulted from thickened metal layer may increase the risk of electrical short-circuiting for optoelectronic devices. In this paper, a TCE of Au-grid embedded in polydimethylsiloxane (PDMS) has been developed by an electrochemical-assisted peeling technique. By a sacrificial etching and transfer process, a smooth surface of Au/PDMS is achieved. The fabricated Au/PDMS TCE shows a surface roughness of 15 nm, a sheet resistance of 8.03 Ω/sq., an optical transmittance of 95.04% and a figure of merit (FoM) of 910. In addition, the mechanical stability of fabricated TCE is also investigated by 10,000 cycles bending with a bending radius of 2 mm. Using the fabricated TCE, a flexible alternating-current-driven electroluminescent (ACEL) device is demonstrated and evaluated, which confirms the use of Au/PDMS TCEs in optoelectronic applications.

1. Introduction

In recent years, many flexible devices including flexible photoelectric devices [1–5], flexible solar cells [6–8], flexible energy collectors [9–11] and portable sensors [12–14] have been proposed and manufactured to meet a wide variety of demands. The flexible transparent conductive electrodes (F-TCEs) are indispensable components in electronic devices. Indium tin oxide (ITO), as one of the most common used oxide-based TCEs, has dominated the optoelectronic markets for years due to its low resistance and high optical transparency. But the intrinsic mechanical property of ITO makes it easily crack at small strains, which limits its employment in the flexible optoelectronic devices such as OLED and OPV. To achieve large flexibility of TCEs, tremendous efforts have been devoted to develop alternative materials such as conductive polymers [15–17], graphene [18–20], carbon nanotubes [21,22] and metal grids [23–25]. Among these alternatives, metal grids have the unique feature of increasing conductivity without influencing transmittance by enlarging the thickness of metal layer. Therefore, appropriate sheet resistance and optical transparent can be simultaneously achieved by optimizing the geometric design of metal grids. Nevertheless, a drawback of increasing the thickness of metal grids is that the surface flatness will increase accordingly, which will restrict the applications in optoelectronic devices.

At present, several fabrication techniques of metal grid F-TCEs have been extensively investigated, such as electron-beam (EB) lithography [26], thermal evaporation [27], and printing technology [28]. However, despite their potential to replace ITO, those methods suffer non-negligible disadvantages more or less. For example, EB lithography is an effective way to define refined micro/nano-patterns, but the technique is expensive and difficult to mass production; thermal evaporation is unfriendly to most flexible organic substrates; printing technology is widely used due to its low cost, simple process and high efficiency, but an additional planarization step is needed to improve the poor surface flatness.

To alleviate the aforementioned problems, we propose a F-TCE structure of Au-grid embedded in polydimethylsiloxane (PDMS) substrate. An electrochemical-assisted peeling method is utilized to transfer the Au/PDMS TCE from a sacrificial stainless foil. Compared with conventional wet or dry etching [29,30], our method shows dramatically accelerated peeling-off speed. Besides, it is much cheaper than the laser-

* Corresponding author at: School of Microelectronics, Southern University of Science and Technology, Shenzhen 518055, China.
E-mail address: wangm@sustech.edu.cn (M. Wang).

https://doi.org/10.1016/j.mee.2021.111511
Received 4 September 2020; Received in revised form 14 November 2020;
Available online 23 January 2021

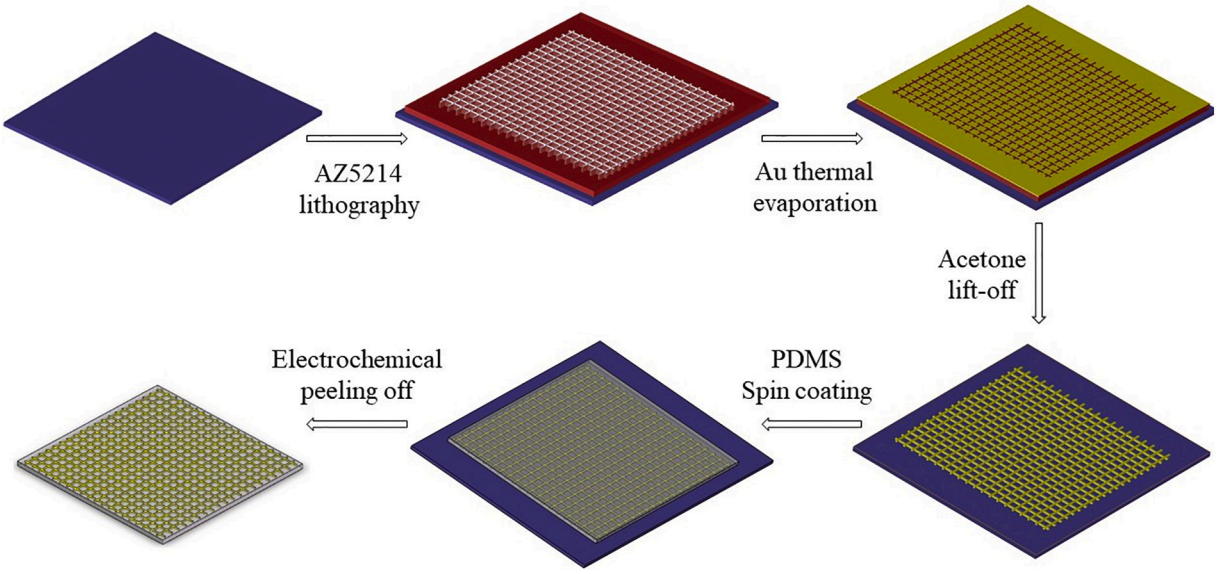

Fig. 1. Fabrication flow of Au/PDMS TCE by electrochemical-assisted peeling.

aided peeling [31]. We investigated the effect of Au-grid designs on the electrical and optical properties of the Au/PDMS TCEs. It is found that when the line width is 5 μm and the grid pitch is 205 μm, the TCE has a sheet resistance of 8.03 Ω/sq. and a transmittance of 95.04%. Meanwhile, a good mechanical stability of the fabricated TCE is demonstrated by a 10,000 bending cycle. An alternating-current-driven electroluminescent (ACEL) device consists an ZnS:Mn/PDMS emission layer and prepared Au/PDMS TCEs was fabricated to test the practical feasibility.

2. Experiments

2.1. Fabrication of Au/PDMS TCE

The fabrication process of Au/PDMS TCE is illustrated in Fig. 1. Firstly, a lift-off process was used to form the grid trenches on stainless substrate. A film of ~2 μm thick AZ5214 (Suzhou Research Materials Microtech Co., Ltd) was spin-coated on a 45 μm thick 304 stainless foil (SUS304, Kunshan Feng Da Co., Ltd). Then the photoresist was pre-

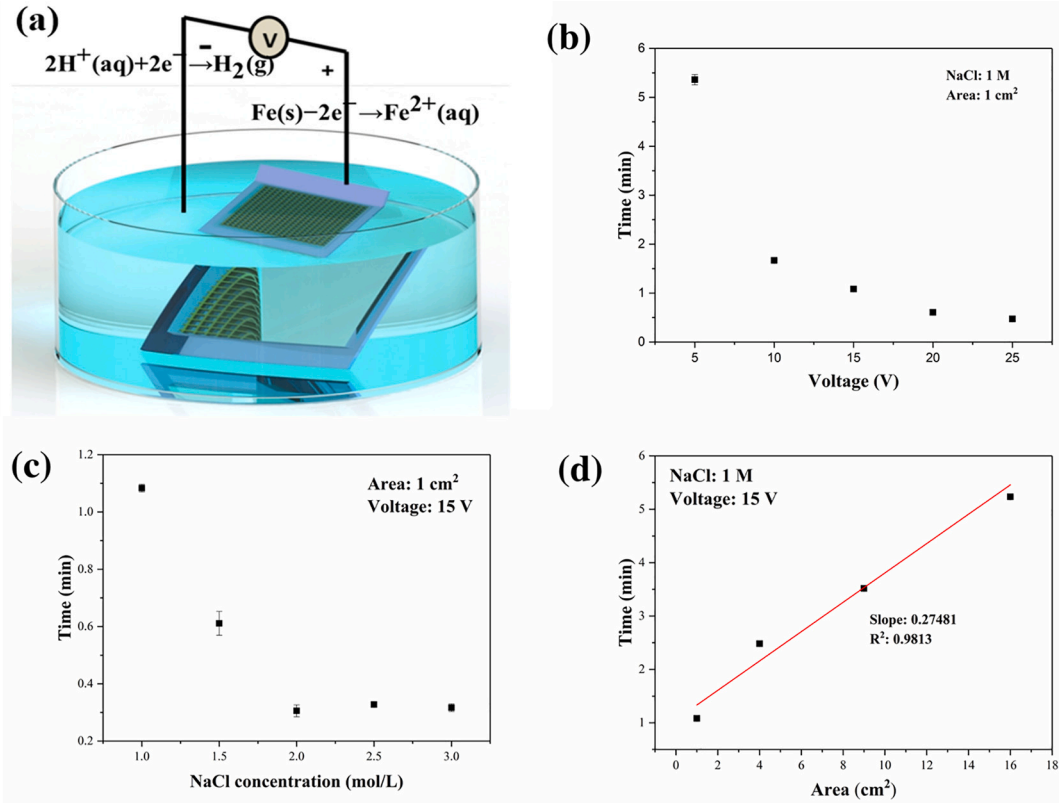

Fig. 2. (a) the schematic illustration of the electrochemical-assisted peeling method. (b)-(d) plots of average delamination time as a function of applied voltage from 5 V to 25 V (b), NaCl concentration from 1 M to 3 M (c) and etch area from 1 cm^2 to 16 cm^2 (d) and with the other two fixed variables addressed in the graphs.

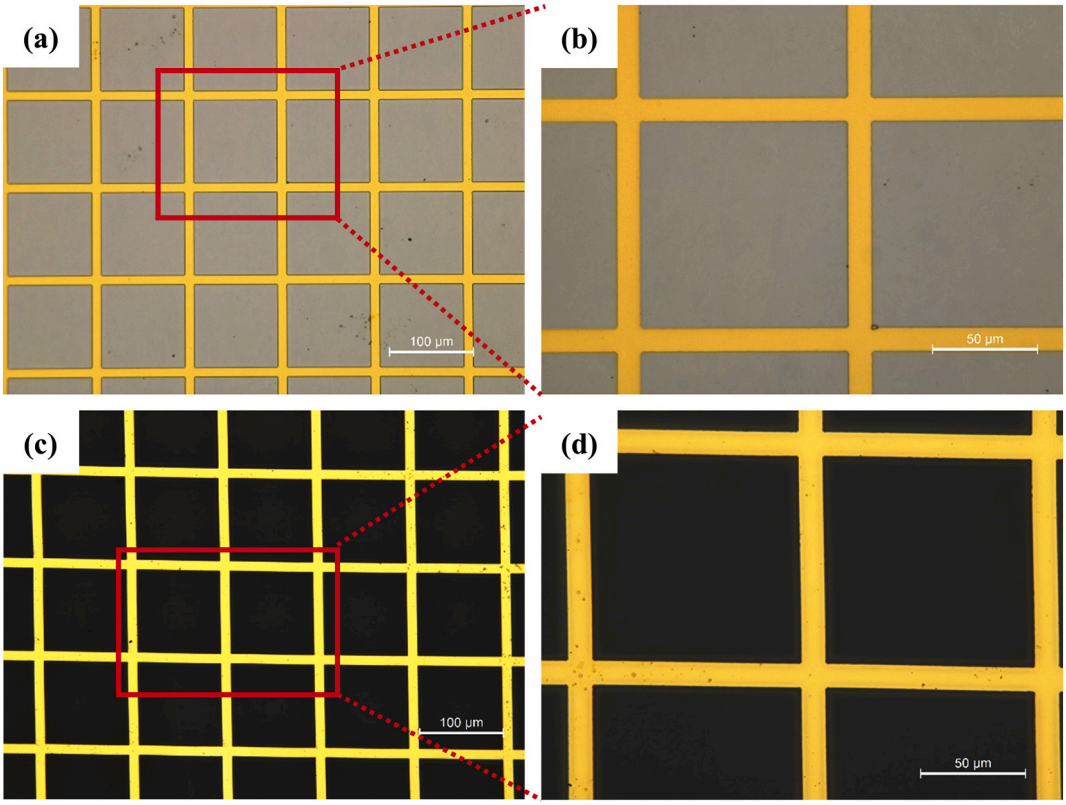

Fig. 3. (a, b) Au-grid (line width = 10 μm, Au-grid pitch = 100 μm, Au-grid thickness = 200 nm) on stainless steel 304 substrate after lift-off and (c, d) the Au-grid embedded in PDMS after peeling.

baked on a hot plate to improve the adhesion to the substrate. After the first exposure of 5 s on the UV exposure machine (Karl SUSS MA/BA 6), the sample was post-baked at 120 °C for 2 min to produce a cross-linking reaction at the exposed area. After a flood exposure, the gridline can be dissolved in development solution to deposit Au in the after step. Then an Au layer with a thickness of 200 nm was deposited by a thermal evaporator (VNANO Vacuum Technology Co., Ltd). Thereafter, the unwanted photoresist and metal were washed away to obtain Au-grid on stainless foil. Secondly, a PDMS layer was deposited to cover the metal grid. The mixed solution with a weight ratio of 1:10 between commercial PDMS solution (Slygard 184, Dow Corning) and curing agent was utilized. The mixture was spin-coated at 1000 rpm for 30 s. Then the sample was vacuumized to extract the air between substrate and PDMS and cured at 120 °C for 30 min in an oven. The thickness of cured PDMS was measured at about 80 μm. Finally, an electrochemical-assisted peeling method was employed to etch stainless steel foil. NaCl aqueous solution was chosen as the electrolyte. To prevent the formation of any precipitate, a small amount of HCl solution was added to control PH of the electrolyte. Positive and negative potentials were applied to the foil and binder clip dipped into the electrolyte, respectively. Consequently, the Au/PDMS TCE was separated from the sacrificial layer without suffering any noticeable mechanical and chemical damages. A delamination yield of 100% was obtained.

2.2. Characterization of TCE

The sheet resistance of fabricated TCE was measured by a four-probe meter (FT-341, Argal Instrument) while its transmittance was obtained on a UV–Vis spectrophotometer (PerkinElmer LAMBDA 750S) in the wavelength range of 400–800 nm. A home-made programable telescopic link equipped with a multimeter was used to observe the resistance while bending. The surface flatness of TCE was measured by a white light interferometer (KLA Zeta 20).

2.3. Fabrication of ACEL device using Au/PDMS

An ACEL device comprised three layers, fabricated TCE/EML/SUS foil, which is a flexible emissive structure. The 4×4 cm^2 SUS substrate was cleaned before emission layer attachment. The cleaning procedure included rinsing in ethanol, acetone and deionized water. Then, a mixture of ZnS:Mn phosphors (Shenzhen Oubaite Technology Co. LTD, 20–45 μm powder) and PDMS with a weight ratio of 7:3 and a curing agent of 10:1 was spin-coated on SUS substrate at 3000 rpm for 15 s, forming an emissive layer (thickness ~ 90 μm). Subsequently, the Au embedded PDMS electrode (thickness ~ 80 μm) using sacrificial etching and transferring processes was gently transferred and attached on top of emissive layer. An additional Ag layer with a thickness of 150 nm was evaporated on the edges of Au/PDMS using a shadow mask to enhance the electrical connection. The active area of the device was 1.5×2.1 cm^2. The fabricated devices were performed under ambient condition without further package.

3. Results and discussion

3.1. Effect of process parameters on delamination

Fig. 2a illustrates the electrochemical delamination process. After connected to the terminals of a direct current, the anode reaction $Fe(s)-2e^- \rightarrow Fe^{2+}(aq)$ is happened on the positively polarized foil, while the cathode reaction $2H+(aq) + 2e- \rightarrow H_2(g)$ is induced on the negatively polarized binder clip. At the onset of delamination process, the electrolyte solution invades the PDMS/stainless interface along the side edge of the foil. During the anode etching of stainless steel, dissolution of the steel generates voids and channels, and these can trigger capillary force that allow the electrolyte to penetrate into the interface and thus speed up the detachment. Since Fe is more reductive than Au, Au/PDMS remains intact before Fe is fully etched, which guarantees the structure

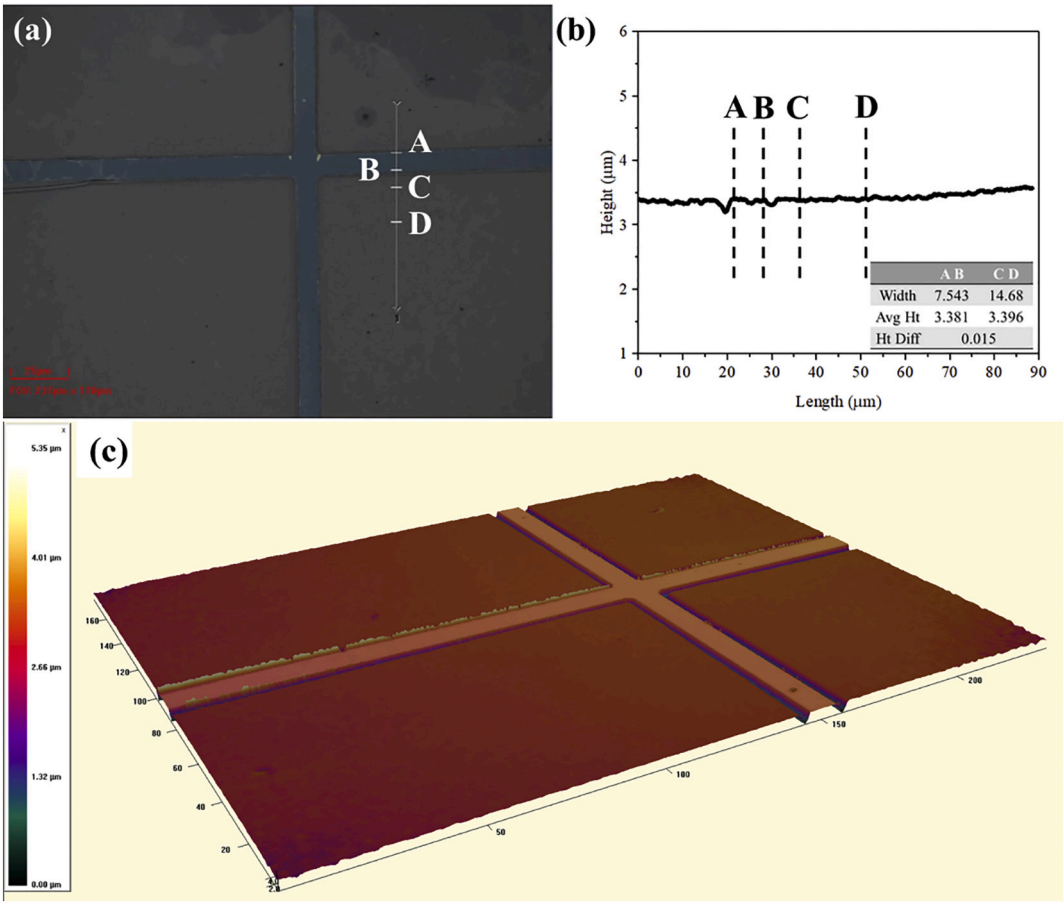

Fig. 4. The results of white light interference of Au/PDMS TCE (line width = 10 μm, Au-grid pitch = 100 μm, line thickness = 200 nm): (a) 2D-geometry, (b)relative height along the white line and (c) 3D-geometry. The inset table shows the width and average height between slash lines (unit: μm).

integrity of transferred TCEs. The proposed electrochemical-assisted delamination process is a simple and rapid transferring technique, which is promising for mass production.

The parameters of the electrochemical process directly affect the detachment speed of Au/PDMS TCEs. The effect of different applied voltages, etching area and electrolyte concentrations on delamination were investigated. The results are shown in Fig. 2b-d. The high voltage and NaCl concentration are conducive to expedite the peeling-off process. As shown in Fig. 2b, the exfoliation speed was gradually maximized and leveled off at 20 V, which means the delamination is restrained by the electrolyte climbing along the interface. The delaminate process can be accelerated by increasing the NaCl concentration, because high electrochemical conductivity can promote the electrochemical reaction. However, when the solution concentration exceeds 2 M, there is basically no rise for the etching speed, as shown in Fig. 2c, which implies the diffusions of reactant and product limit further etching. The delamination attains an average time of 0.6 min at 15 V using 1 M NaCl and 1 cm^2 etching area. The electrochemical-assisted delamination is quite faster than that of conventional wet etching, which usually takes tens of minutes. Additionally, the working voltage of 15 V is much larger than the standard electromotive force of Au (−1.7 V). To prevent Au from damage, a voltage cut-off should be adopted before the steel is completely removed. The residual steel is washed away by an additional treatment in HCl solution. Besides, the delamination process for different etching area is produced by using 15 V voltage and 1 M NaCl. A linear relationship between etching rate and etching area is obtained in Fig. 2d.

3.2. Au/PDMS TCE transferring

Fig. 3a and 3b show the Au-grid on stainless steel after lift-off process. Well-patterned Au-grids is obtained. Fig. 3c and 3d depict Au-grid embedded in PDMS after peeling off from stainless steel, and a good reservation of the sheet structure is also demonstrated.

To verify the surface flatness of Au-grid, white light interference is utilized. Because PDMS is transparent, a thin metal layer with a thickness of several nanometers is sputtered on the sample. As shown in Fig. 4, a relatively small height difference of 15 nm is observed between Au-grid and PDMS, which suggests that the Au wires are well implanted in PDMS. Accordingly, a good flatness can be guaranteed by the sacrificial electrochemical-assisted etching method. As shown in 3D-geometry (Fig. 3c), a height difference of about 4 μm between left and right sides is observed, which is caused by the unevenness of the sample placement on the macro level. Moreover, the glitch at the junction of the gold wire and PDMS is about 5 μm high, which may result from the swelling of PDMS during the reaction of electrochemical corrosion separation [32–34]. The swelling can be minimized by modifying the thickness and composition of PDMS.

3.3. Conductivity and transmittance investigation

For the TCEs, the optical transmittance and sheet resistance are the two most important parameters. For metal grid TCEs, the conductivity and transmittance are related to the sheet parameters like grid pitch, line width and line thickness [35]. It is suggested that the transmittance and sheet resistance of the metal grid can be calculated by a filling factor (*FF*) with the following equations.

Table 1
Electrical and optical properties of Au/PDMS TCEs.

Line width/ μm	Au-grid pitch/ μm	Calculated transmittance/%	Experimental transmittance/% (At 550 nm)	Calculated sheet resistance/ Ω/sq	Experimental sheet resistance/ Ω/sq	FoM
5	105	90.70	89.92	4.00	3.94	876
5	205	95.18	95.04	7.72	8.03	910
10	110	82.64	79.43	2.14	2.10	735
10	210	90.70	89.50	4.00	4.00	826

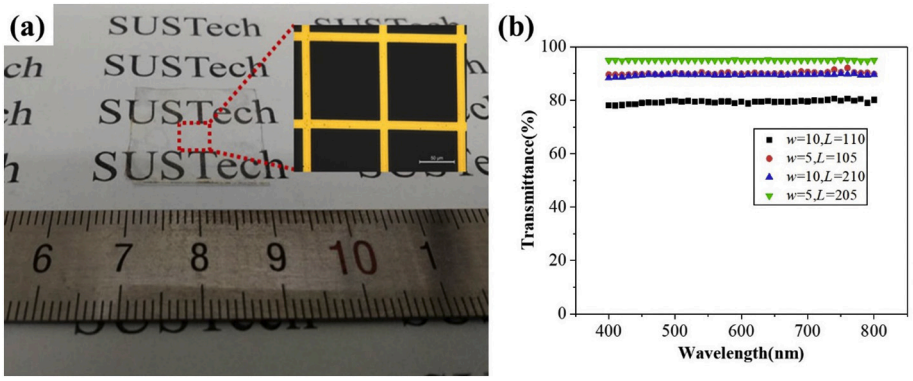

Fig. 5. (a) Optical microscope image of Au/PDMS TCE prepared by electrochemical peeling method and (b) the transmittance of Au/PDMS TCEs in the wavelength range from 400 to 800 nm.

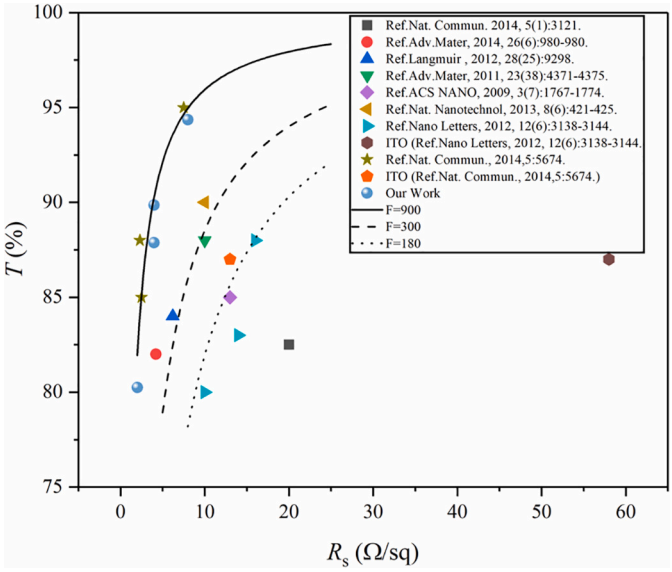

Fig. 6. Comparison of our TCEs and former researches' ones, where the blue balls depict our TCEs. The line and dashed lines from left to right represent a figure-of-merit equal to 700, 300 and 180, respectively.

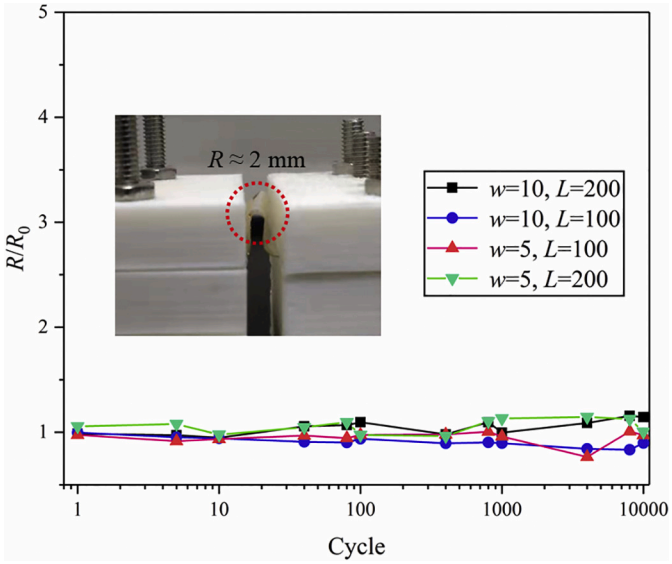

Fig. 7. Resistance variations after bending the cycling tests for different Au/PDMS TCEs (bending radius: 2 mm). The inset shows the picture of bending.

$$FF = \frac{(L \times w) + [(L - w) \times w]}{L^2} \tag{1}$$

$$T = 1 - FF \tag{2}$$

$$R_s = \xi \frac{\rho}{h} \times \frac{1}{FF} \tag{3}$$

where L and w are Au-grid pitch and the width of Au-grid line, as described in Fig. 3. T and R_s are transmittance at 550 nm and sheet resistance, respectively. ρ is the resistivity of metal (data for bulk Au is used in this study), h is the metal line thickness (200 nm), and ξ is a correction factor, which is related to experiment conditions and can be determined experimentally for a given deposition technique and specific process [35,36]. The ratio of electrical conductance to optical transmittance, so-called the figure-of-merit (FoM) of TCEs, can be calculated using the following equation.

$$FoM = \frac{188.5}{R_s\left(\frac{1}{\sqrt{T}} - 1\right)} \tag{4}$$

In our experiments, four different Au-grids are designed and fabricated, and the theoretically predicted properties and the measured ones are listed in Table 1. The optical transmissions of different TCEs are shown in Fig. 5. It indicates that transmittance increase with the decreasing Au line width and the increasing Au-grid pitch, while the resistance decrease with the increasing Au line width and the decreasing

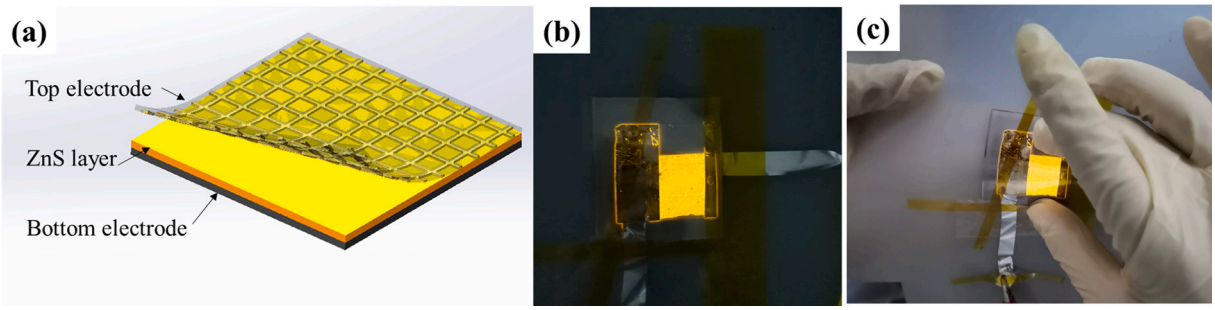

Fig. 8. Electroluminescence device (a) schematic image, (b) operating under flat state and (c) operating under curved state.

Au-grid pitch. The different changing trends between transmittance and resistance suggest a compromise should be made to achieve high transmittance and low resistance simultaneously. Moreover, the varying tendency of experimental results is well consistent with the predicted ones. The differences may result from the variations in grid dimension and material resistivity.

Fig. 6 shows a comparison between our fabricated TCEs and former researches' ones. The FoM as high as 910 is obtained by our TCE when the line width is 5 μm and the grid pitch is 205 μm. Such good electrical and optical properties of Au/PDMS TCEs implies the promising application to the flexible optoelectronic devices.

3.4. Flexibility measurement

Mechanical stability of Au/PDMS TCEs is also investigated. The R/R_0 ratio (R_0 is the initial sheet resistance and R is the sheet resistance after bending) is demonstrated in Fig. 7. In the experiment, Au/PDMS TCEs with an area of 2×2 cm^2 are bended with a bending radius of 2 mm, as shown in the inset to Fig. 7. The resistance variations less than 30% are observed after 10,000 bending cycles for different TCEs, suggesting a good bending robustness. From the video (supporting information), we can see that the resistance of the TCE remains almost unchanged during bending cycles, which implies that the effect of metal buckling on conductivity of Au/PDMS TCE is negligible.

3.5. Application of Au/PDMS as the electrode in ACEL device

To demonstrated that the developed Au/PDMS TCE are compatible with ACEL device and to evaluate the performance, an ACEL device on 4×4 cm^2 stainless substrate is fabricated. The detailed fabrication is illustrated in experimental Section 2.3 and the schematic diagram of the ACEL device is shown in Fig. 8a. The assembled device is efficiently pumped by applying an AC voltage (electric field E = 9.5 V/μm at 5 kHz) as revealed by the ON states. Fig. 8b and c present the operating ACEL device at flattening state and bended state, respectively. The uniform electroluminescence properties under different working conditions were obtained, which suggests that the Au/PDMS electrode is promising for the flexible optoelectronic application. In addition, the uniform electroluminescence implies that the electrode has good surface flatness, especially at the curved state.

4. Conclusions

In summary, the electrochemical-assisted transferred Au/PDMS TCEs have been prepared. Au/PDMS TCEs can be fully delaminated from SUS foil by electrochemical-assisted peeling method. Meanwhile, there is no obvious mechanical and chemical damages in the fabricated Au/PDMS TCEs. A low surface roughness (~15 nm) of Au/PDMS was obtained by casting PDMS on Au grids and sacrificially etching stainless foil. The fabricated Au/PDMS TCEs exhibited high optical transmittance of 95.04%, low resistance of 8.03 Ω/sq., a FoM of 910, and good mechanical stability. Furthermore, a flexible alternating-current-driven electroluminescent (ACEL) device was demonstrated using the fabricated Au/PDMS TCE. The good performances of the device under flattening and curved operating states suggest the promising application of Au/PDMS TCEs to optoelectronic devices.

Supplementary data to this article can be found online at https://doi.org/10.1016/j.mee.2021.111511.

Credit author statement

Min Wang conceived and designed the research. Gang Wang and Yufei Zhai contributed equally to this work. Gang Wang and Yu Fei Zhai carried out experiments and performed the testing. Chenghao Lv and Wenjing Fan performed metal deposition, fabricated the ACEL device and took the SEM and optical images. Cong Zhao assisted with the luminescence testing. All authors participated in drafting the manuscript, discussion and interpretation of the data.

CRediT authorship contribution statement

Gang Wang: Conceptualization, Investigation, Writing - original draft. **Yufei Zhai:** Data curation, Writing - review & editing. **Chenghao Lv:** Data curation. **Wenjing Fan:** Methodology. **Cong Zhao:** Investigation. **Min Wang:** Writing - review & editing, Supervision.

Declaration of Competing Interest

The authors declared that they have no conflicts of interest to this work. We declare that we do not have any commercial or associative interest that represents a conflict of interest in connection with the work submitted.

Acknowledgements

This work was supported by the Natural Science Foundation of China (Grant No. 61805114), the Natural Science Foundation of Guangdong Province (Grant No. 2018A030310123).

References

[1] T.H. Han, Y. Lee, M.R. Choi, et al., Extremely efficient flexible organic light-emitting diodes with modified graphene anode[J], Nat. Photonics 6 (2) (2012) 105–110.
[2] M.S. White, M. Kaltenbrunner, E.D. Glowacki, et al., Ultrathin, highly flexible and stretchable PLEDs[J], Nat. Photonics 7 (10) (2013) 811–816.
[3] S.P. Pang, Y. Hernandez, X.L. Feng, et al., Graphene as transparent electrode material for organic electronics[J], Adv. Mater. 23 (25) (2011) 2779–2795.
[4] F. Bonaccorso, Z. Sun, T. Hasan, et al., Graphene photonics and optoelectronics[J], Nat. Photonics 4 (9) (2010) 611–622.
[5] S. Jung, S. Lee, M. Song, et al., Extremely flexible transparent conducting electrodes for organic devices[J], Adv. Energy Mater. 4 (1) (2014) 1–8.
[6] C.C. Lin, Y.J. Chuang, W.H. Sun, et al., Ultrathin single-crystalline silicon solar cells for mechanically flexible and optimal surface morphology designs[J], Microelectron. Eng. 145 (SEP.1) (2015) 128–132.
[7] L.G. De Arco, Y. Zhang, C.W. Schlenker, et al., Continuous, highly flexible, and transparent graphene films by chemical vapor deposition for organic photovoltaics [J], ACS Nano 4 (5) (2010) 2865–2873.

[8] W. Cao, Y. Zheng, Z. Li, et al., Flexible organic solar cells using an oxide/metal/oxide trilayer as transparent electrode[J], Org. Electron. 13 (11) (2012) 2221–2228.
[9] T.S.V.D. Heever, W.J. Perold, The performance of nanogenerators fabricated on rigid and flexible substrates[J], Microelectron. Eng. 112 (Dec.) (2013) 41–45.
[10] Y. Hu, L. Lin, Y. Zhang, et al., Replacing a battery by a nanogenerator with 20 V output[J], Adv. Mater. 24 (1) (2012) 110–114.
[11] G.-T. Hwang, V. Annapureddy, J.H. Han, et al., Self-powered wireless sensor node enabled by an aerosol-deposited PZT flexible energy harvester[J], Adv. Energy Mater. 6 (13) (2016) 1600237.
[12] C.C. Yeh, S.H. Lo, M.X. Xu, et al., Fabrication of a flexible wireless pressure sensor for intravascular blood pressure monitoring[J], Microelectron. Eng. 213 (15) (2019) 55–61.
[13] M. Zhang, S. Guo, D. Weller, et al., CdSSe nanowire-chip based wearable sweat sensor[J], J. Nanobiotechnol. 17 (1) (2019) 42.
[14] S.H. Wang, J. Xu, W.C. Wang, et al., Skin electronics from scalable fabrication of an intrinsically stretchable transistor array[J], Nature 555 (7694) (2018) 83–88.
[15] N. Kim, H. Kang, J.H. Lee, et al., Highly conductive all-plastic electrodes fabricated using a novel chemically controlled transfer-printing method[J], Adv. Mater. 27 (14) (2015) 2317–2323.
[16] M. Kaltenbrunner, M.S. White, E.D. Glowacki, et al., Ultrathin and lightweight organic solar cells with high flexibility[J], Nat. Commun. 3 (2012) 770.
[17] V. Ratautaite, G. Bagdziunas, A. Ramanavicius, et al., An application of conducting polymer polypyrrole for the design of electrochromic pH and CO2 sensors[J], J. Electrochem. Soc. 166 (6) (2019) B297–B303.
[18] J. Woerle, H. Rost, Roll-to-roll production of transparent conductive films using metallic grids[J], MRS Bull. 36 (10) (2011) 789–793.
[19] N. Wang, J. Liu, Y. Zhao, et al., High-performance asymmetric micro-supercapacitors based on electrodeposited MnO2 and N-doped graphene[J], Nanotechnology 30 (23) (2019) 235403.
[20] M. Mohammadnezhad, G.S. Selopal, N. Alsayyari, et al., CuS/graphene nanocomposite as a transparent conducting oxide and Pt-free counter electrode for dye-sensitized solar cells[J], J. Electrochem. Soc. 166 (5) (2018) H3065–H3073.
[21] H.-Z. Geng, K.K. Kim, K.P. So, et al., Effect of acid treatment on carbon nanotube-based flexible transparent conducting films[J], J. Am. Chem. Soc. 129 (25) (2007) 7758–7759.
[22] A. Ben Tahar, A. Romdhane, N. Lalaoui, et al., Carbon nanotube-based flexible biocathode for enzymatic biofuel cells by spray coating[J], J. Power Sources 408 (2018) 1–6.
[23] S. De, T.M. Higgins, P.E. Lyons, et al., Silver nanowire networks as flexible, transparent, conducting films: extremely high DC to optical conductivity ratios[J], ACS Nano 3 (7) (2009) 1767–1774.
[24] D.S. Leem, A. Edwards, M. Faist, et al., Efficient organic solar cells with solution-processed silver nanowire electrodes[J], Adv. Mater. 23 (38) (2011) 4371–4375.
[25] H. Jung, H. Go, G.C. Park, et al., Silver nanowire-based stretchable transparent electrode for flexible organic light-emitting diode[J], J. Nanosci. Nanotechnol. 19 (4) (2019) 2044–2048.
[26] S. Jung, S. Lee, M. Song, et al., Extremely flexible transparent conducting electrodes for organic devices[J], Adv. Energy Mater. 4 (1) (2014) 1–8.
[27] Guo C F and Ren Z F. Flexible transparent conductors based on metal nanowire networks [J]. Mater. Today, 18(3), 143–154.
[28] Meng X., Hu X., Yang X., et al. Roll-to-roll printing of meter-scale composite transparent electrodes with optimized mechanical and optical properties for photoelectronics [J]. ACS Appl. Mater. Interfaces, 10(10), 8917–8925.
[29] M.H. Seo, J.-Y. Yoo, S.-Y. Choi, et al., Versatile transfer of an ultralong and seamless nanowire array crystallized at high temperature for use in high-performance flexible devices[J], ACS Nano 11 (2) (2017) 1520–1529.
[30] H. Fang, J.N. Zhao, K.J. Yu, et al., Ultrathin, transferred layers of thermally grown silicon dioxide as biofluid barriers for biointegrated flexible electronic systems[J], Proc. Natl. Acad. Sci. U. S. A. 113 (42) (2016) 11682–11687.
[31] K.I. Park, J.H. Son, G.T. Hwang, et al., Highly-efficient, flexible piezoelectric PZT thin film nanogenerator on plastic substrates[J], Adv. Mater. 26 (16) (2014) 2514–2520.
[32] R. Dangla, F. Gallaire, C.N. Baroud, Microchannel deformations due to solvent-induced PDMS swelling, Lab Chip 10 (21) (2010) 2972–2978.
[33] L.E.M. Gevers, I.F.J. Vankelecom, P.A. Jacobs, Solvent-resistant nanofiltration with filled polydimethylsiloxane (PDMS) membranes, J. Membr. Sci. 278 (1) (2006) 199–204.
[34] N. Stafie, D.F. Stamatialis, M. Wessling, Effect of PDMS cross-linking degree on the permeation performance of PAN/PDMS composite nanofiltration membranes, Sep. Purif. Technol. 45 (3) (2005) 220–231.
[35] Y. Jang, J. Kim, D. Byun, Invisible metal-grid transparent electrode prepared by electrohydrodynamic (EHD) jet printing[J], J. Phys. D Appl. Phys. 46 (15) (2013) 155103.
[36] D.S. Ghost, T.L. Chen, V. Pruneri, High figure-of-merit ultrathin metal transparent electrodes incorporating a conductive grid [J], Appl. Phys. Lett. 96 (4) (2010), 041109.